Int. J. Electrochem. Sci., 12 **(2017)** 10471 – 10483, doi: 10.20964/2017.11.42

International Journal of
ELECTROCHEMICAL
SCIENCE
www.electrochemsci.org

High-Performance N-doped Bifunctional Carbon Electrocatalysts Derived from Polymer Waste for Oxygen Reduction and Evolution Reaction

Jinjin Xuan, Ziwu Liu[*]

Low Carbon Energy Institute and School of Chemical Engineering, China University of Mining & Technology, Xuzhou 221008, Jiangsu, China
[*]E-mail: lzwmsy@cumt.edu.cn

Received: 12 June 2017 / *Accepted:* 4 September 2017 / *Published:* 12 October 2017

Developing novel bifunctional heteroatom-doped carbon electrocatalysts for the oxygen reduction reaction (ORR) and oxygen evolution reaction (OER) is vital for the development of fuel cells, metal-air batteries and water oxidation systems. Herein, a nitrogen (N)-containing polymer waste was collected and used to synthesize N-doped bifunctional carbon electrocatalysts (N-BCEs). The results indicated that the N-containing polymer waste from a living environment can be converted to N-BCEs easily. In addition, the surface areas, pore structures and N doping contents of N-BCEs were further optimized by cyanoguanidine. Most importantly, the electrochemical tests demonstrated that the as-prepared N-BCEs exhibited comparable ORR and OER activities to the commercial noble-metal Pt-C and IrO_2 electrocatalysts in both acidic and alkaline media, indicating that environmentally-unfriendly heteroatom-containing polymer wastes can be utilized to synthesize advanced heteroatom-doped BCEs for ORR and OER in future fuel cells, metal-air batteries and water oxidation.

Keywords: N-containing polymer wastes; bifunctional electrocatalysts; oxygen reduction reaction; oxygen evolution reaction; electrocatalysis

1. INTRODUCTION

The oxygen reduction reaction (ORR) and oxygen evolution reaction (OER) are two very active research topics in the field of the energy storage and conversion for use in fuel cells, batteries and water oxidation systems due to their critical roles in the electrochemical performances of these systems. For these two key reactions, presently, one giant challenge is to develop more effective and much cheaper bifunctional electrocatalysts to ameliorate the O_2 reduction and evolution efficiencies [1]. For ORR/OER bifunctional electrocatalysts, considerable attention has mainly focused on the

design of noble metal or metal oxide, hydroxide and chalcogenide electrocatalysts in the past years [2-9]. Although great progress has been made, most of the developed ORR/OER bifunctional metal-based electrocatalysts still exist some obvious flaws such as high cost, low selectivity or poor stability [1], which have hindered their practical application in energy storage and conversion devices. Fortunately, recently, many advancements have demonstrated that metal-free carbon materials containing foreign atoms exhibit much higher ORR/OER activities in both acidic and alkaline media [10-16], showing great promise to replace metal-based ORR/OER bifunctional electrocatalysts. However, for these novel metal-free heteroatom-doped bifunctional carbon electrocatalysts (BCEs), their large-scale application is inaccessible currently because the heteroatom precursors mainly employed to fabricate BCEs are flammable, explosive, toxic and high-cost synthetic chemicals [17]. To reduce the excessive dependence on these synthetic chemicals and develop lower-cost and more effective BCEs for large-scale applications, in this work, we rationally selected a low-cost and nitrogen-rich polymer waste (PW) as a N precursor to prepare cost-effective and high-performance N-doped bifunctional carbon electrocatalysts (N-BCEs). The results showed that the selected cheap polyamide 66 (PA66) could be converted into N-doped porous carbon materials easily. In addition, their surface areas, pore structures and N doping contents were further optimized by mixing PA66 with low-cost cyanoguanidine. Most importantly, electrochemical tests indicated that the as-prepared N-BCEs exhibited comparable ORR and OER activities to noble-metal catalysts in both acidic and alkaline media, showing great promise for applications in future energy storage and conversion devices, especially in regenerative fuel cells and rechargeable metal-air batteries. It is noted that utilizing a low-cost and N-containing polymer waste to fabricate novel BCEs with controllable doping has rarely been reported.

2. EXPERIMENTAL SECTION

2.1 Preparation of materials

In a typical experiment, 8.0 g of the selected N-containing PA66 was placed into a 100.0 mL hydrothermal reactor with 70.0 mL of deionized water. The mixture was heated at 180.0 ℃ for 4.0 h and then filtered. The obtained solid PA66 was pulverized after drying at 50.0 ℃ for 5.0 h and 4.0 g of powder was mixed with 0.4 g of $Fe_2(SO_4)_3$. Then, the mixture was heated at 700.0 ℃ for 2.0 h and 900.0 ℃ for 1.0 h in a tubular furnace according to Ref. 17. The resulting sample was collected and denoted as N-BCE1. N-BCE2, N-BCE3, N-BCE4 and N-BCE5 were prepared according to the mass ratios of 1 : 6, 1 : 12, 1 : 20 and 0 : 1 of PA66 to cyanoguanidine, respectively, with 0.4 g of $Fe_2(SO_4)_3$ as a catalyst under the same synthesis conditions.

2.2 Electrode preparation and electrochemical experiments

The glassy carbon electrode (GC, 5.0 mm in diameter) preparation was based on Ref. 17. Electrochemical experiments were carried out at room temperature in a three-electrode cell connected to an electrochemical analyzer (Pine Research Instrumentation, USA). N-BCE1/GC, N-BCE2/GC, N-BCE3/GC, N-BCE4/GC, N-BCE5/GC and Pt–C/GC were used as the working electrodes, Ag/AgCl

with saturated KNO_3 was used as the reference electrode, and a Pt or graphite electrode was used as the counter electrode. All potentials were measured vs. the potential of the Ag/AgCl electrode and converted to the reversible hydrogen electrode (RHE) through the equation of $V_{RHE} = V_{Ag/AgCl} + V_{Ag/AgCl\ vs\ NHE} + 0.0592pH$ (NHE is the normal hydrogen scale; $V_{Ag/AgCl\ vs\ NHE}$ is 0.1976; pH is 13 or 1 in 0.1 M KOH or 1.0 M $HClO_4$ solution, respectively). The cyclic voltammetry (CV) experiments were conducted in an oxygen-saturated 0.1 M KOH or 1.0 M $HClO_4$ solution at room temperature. The linear sweep voltammetry (LSV) measurements were performed in an oxygen-saturated 0.1 M KOH or 1.0 M $HClO_4$ solution at a scan rate of 10.0 mV s^{-1}. The OER current densities of the samples were estimated by LSV in a nitrogen-saturated 0.1 M KOH or 1.0 M $HClO_4$ solution in the potential range of 0.0 to +0.9 V or +0.5 to +1.3 V at a rotation speed of 1600.0 rpm and scan rate of 10.0 mV s^{-1}. The loaded amount of each example on the surface of the bare GC was 0.153 mg cm^{-2}.

The Koutecky-Levich plots were obtained by $I^{-1} = Ik^{-1} + (0.62nFCD^{2/3}v^{-1/6}\omega^{1/2})^{-1}$, where Ik^{-1} is the kinetic current density, ω is the rotational speed, n is the number of electrons transferred, F is the Faraday constant (F = 96485.0 C mol^{-1}), C is the bulk concentration of O_2 (C = 1.2×10^{-3} mol L^{-1} for 0.1 M KOH; C = 1.6×10^{-3} mol L^{-1} for 1.0 M $HClO_4$), D is the diffusion coefficient of O_2 (D = 1.9×10^{-5} cm^2 s^{-1} for 0.1 M KOH; D = 1.1×10^{-5} cm^2 s^{-1} for 1.0 M $HClO_4$), v is the kinetic viscosity of the electrolyte (0.01 cm^2 s^{-1} for both 0.1 M KOH and 1.0 M $HClO_4$), ω is the angular velocity of the disk ($\omega = 2.0\pi N$, N is the linear rotation speed). The n values were calculated by the following equation: n = 4ID / (ID + IR/N), where N is the collection efficiency with a value of 0.37, and ID and IR are the faradaic-disk and faradaic-ring currents, respectively.

2.3 Characterizations

The morphologies of the samples and elemental compositions were characterized by scanning electron microscopy (SEM, ZEISS Merlin) and high resolution transmission electron microscopy (HRTEM, JEOL 2010F) operating at 200 kV. The surface areas, pore volumes and pore size distributions of the samples were measured by the Brunauer–Emmett–Teller (BET, Autosorb IQ) method. Elemental compositions were analyzed on a vario MACRO cube CHNS elemental analyzer. X-ray photoelectron spectroscopy (XPS) measurements were performed on a Thermo Scientific ESCALAB 250XI using Al Kα radiation, and the C1s peak at 284.8 eV was used as an internal standard.

3. RESULTS AND DISCUSSION

SEM and TEM images (Fig. 1A-1F) illustrated that PW-based N-BCE1, N-BCE2, N-BCE3 and N-BCE4 were composed of porous carbon, and N-BCE5 synthesized with cyanoguanidine consisted of porous and tube carbon compositions. The hysteresis loops in the N_2 adsorption-desorption isotherms and porous size distributions (Fig. 2A-2B) confirmed that all the prepared samples contained mesoporous structures. The surface areas (260.6, 383.6 and 353.3 m^2 g^{-1}) of N-BCE2, N-BCE3 and N-

BCE4 were much larger than those (30.1 and 139.2 m^2 g^{-1}) of N-BCE1 and N-BCE5, indicating that the mixing of PA66 and cyanoguanidine could increase the surface area. The elemental analyses (Fig. 1A-1E) showed that the N contents (3.72, 3.06 and 2.88 wt.%) in N-BCE2, N-BCE3 and N-BCE4 were much larger than those (1.55 and 1.59 wt.%) of N-BCE1 and N-BCE5, indicating that the addition of cyanoguanidine also ameliorated the N doping level. The XPS analyses of N-BCE1, N-BCE3 and N-BCE5 (Fig. 2C-2F) confirmed the successful N doping. Four N species of pyridinic N (ca. 398.1 eV), graphitic N (ca. 400.8 eV), pyrrolic N (ca. 399.2 eV) and oxidized N (ca. 401.9 eV) were identified from the N1s peaks at approximately 400 eV [17,18]. The pyridinic N contribution (31.1 at.%) in N-BCE3 was much larger than those (20.5 and 26.4 at.%) in N-BCE1 and N-BCE5. However, the graphitic N contribution (46.5 at.%) in N-BCE3 was much smaller than those (54.1 and 48.2 at.%) in N-BCE1 and N-BCE5. The pyrrolic N contribution (11.2 at.%) in N-BCE3 was similar than that (6.7 at.%) in N-BCE5 and smaller than that (21.3 at.%) in N-BCE1. The oxidized N contribution (11.3 at.%) in N-BCE3 was smaller than that (18.6 at.%) in N-BCE5 and larger than that (4.0 at.%) in N-BCE1. Meanwhile, since $Fe_2(SO_4)_3$ was used as catalyst in this work, Fe2p peaks were also found in the XPS spectra (Fig. 2C). The Fe2p peaks at ca. 706.6, 720.0, 712.0, 724.0, 710.7 and 725.2 eV were assigned to $Fe^{o}2p_{3/2}$, $Fe^{o}2p_{1/2}$, $Fe^{2+}2p_{3/2}$, $Fe^{2+}2p_{1/2}$, $Fe^{3+}2p_{3/2}$ and $Fe^{3+}2p_{1/2}$, respectively [18,19].

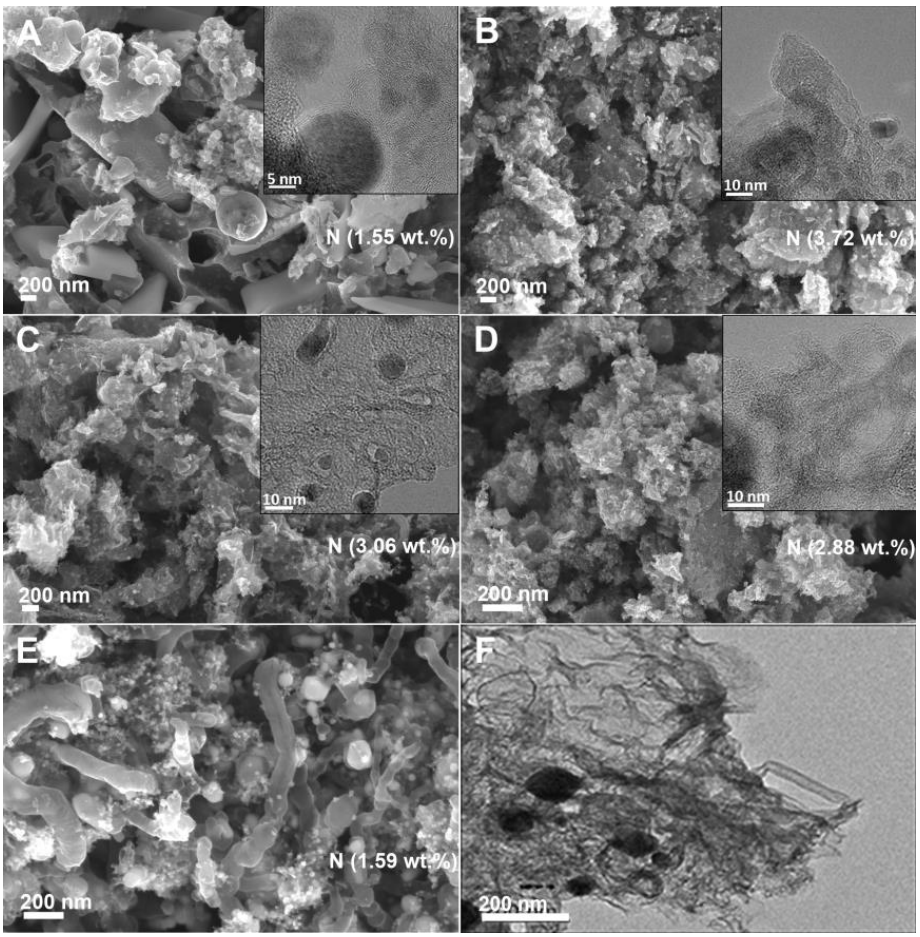

Figure 1. The SEM and TEM images of N-BCE1 (A), N-BCE2 (B), N-BCE3 (C), N-BCE4 (D) and N-BCE5 (E, F), and the N content inserted in each corresponding SEM image.

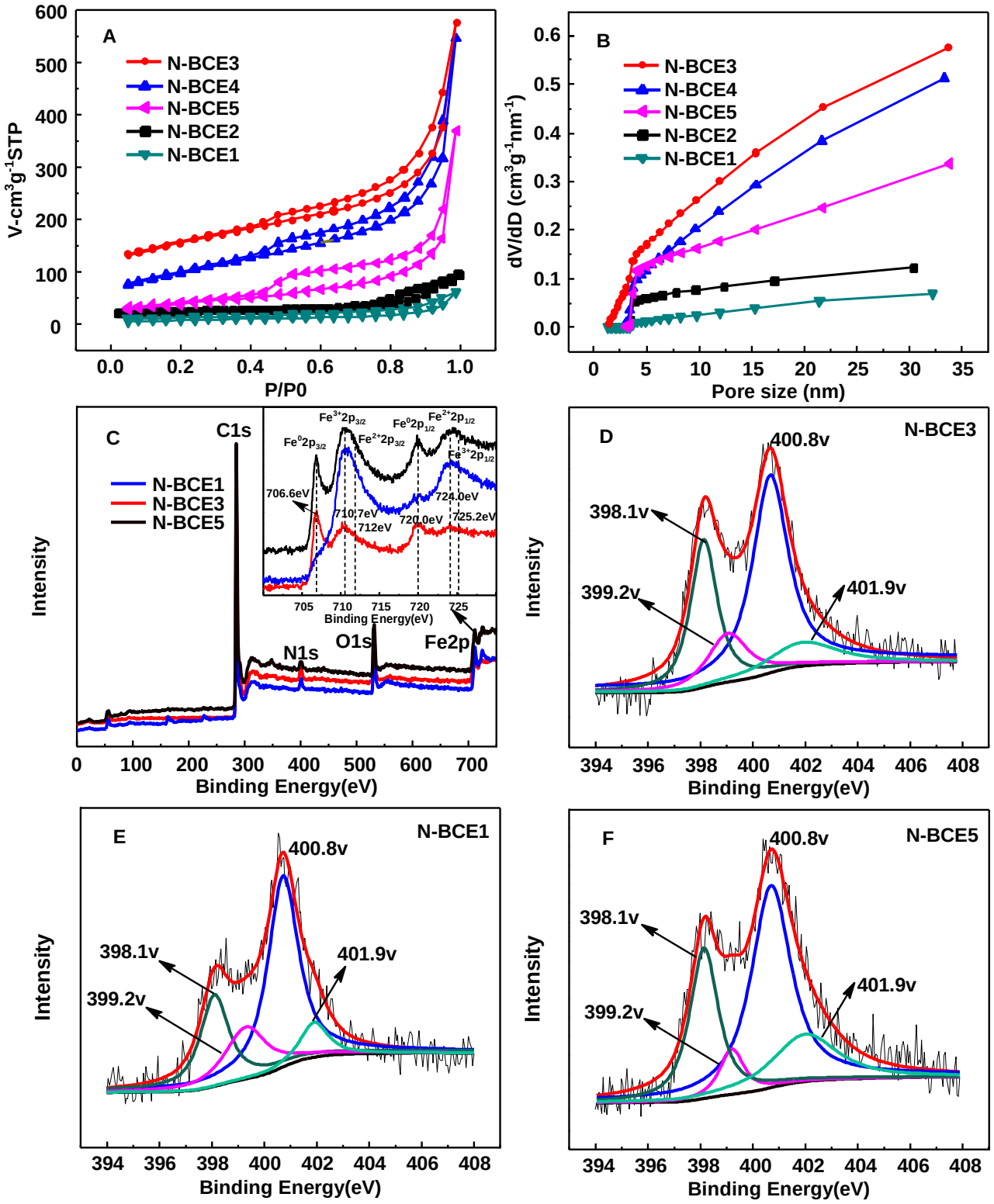

Figure 2. The N_2 sorption isotherms of N-BCE1, N-BCE2, N-BCE3, N-BCE4 and N-BCE5 (A) and their pore size distributions (B). XPS surveys of N-BCE1, N-BCE3 and N-BCE5 and Fe2p spectra (C). The N1s spectra of N-BCE1, N-BCE3 and N-BCE5 (D-F).

To investigate the electrocatalytic activity for ORR, the CV measurements were performed in O_2 saturated 0.1 M KOH. The test results in Fig. 3A indicate that N-BCE2, N-BCE3 and N-BCE4 displayed strikingly improved ORR activity when compared with N-BCE1. Among the five samples, N-BCE3 with a peak current of 3.38 mA cm^{-2} at 0.717 V exhibited superior ORR activity in alkaline medium. The remarkable ORR activity of N-BCE3 was also observed from the CVs in acidic medium. As shown in Fig. 3B, N-BCE3 with a peak current of 4.79 mA cm^{-2} at 0.498 V displayed the best ORR activity as well.

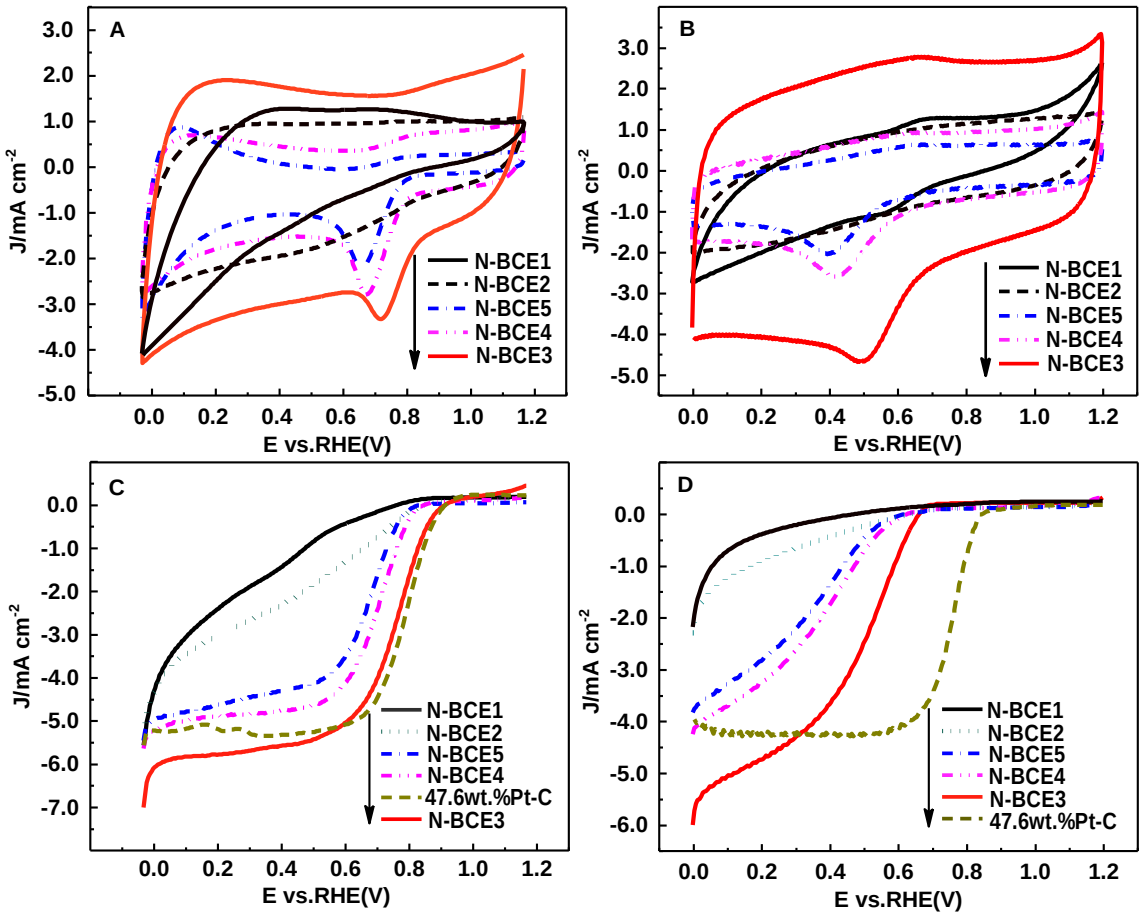

Figure 3. The typical CVs of N-BCE1, N-BCE2, N-BCE3, N-BCE4 and N-BCE5 in O_2-saturated 0.1 M KOH (A) or 1.0 M $HClO_4$ (B) solution. The LSVs of N-BCE1, N-BCE2, N-BCE3, N-BCE4, N-BCE5 and commercial Pt–C catalyst in O_2-saturated 0.1 M KOH (C) or 1.0 M $HClO_4$ (D) solution at a rotation speed of 1600.0 rpm.

These results indicate that the N-containing PW can be utilized to prepared effective ORR electrocatalysts by adding a certain amount of cyanoguanidine. Moreover, the superior ORR activity of N-BCE3 was further evidenced by LSV measurements in both oxygen-saturated 0.1 M KOH and 1.0 M $HClO_4$ solutions at a rotation speed of 1600.0 rpm. In alkaline medium, as seen from Fig. 3C, the onset potential and current density for the N-BCE3 were obviously much higher than those for N-BCE1, N-BCE2, N-BCE4 and N-BCE5. Meanwhile, in acidic medium, as shown in Fig. 3D, N-BCE3 also exhibited superior ORR activity.

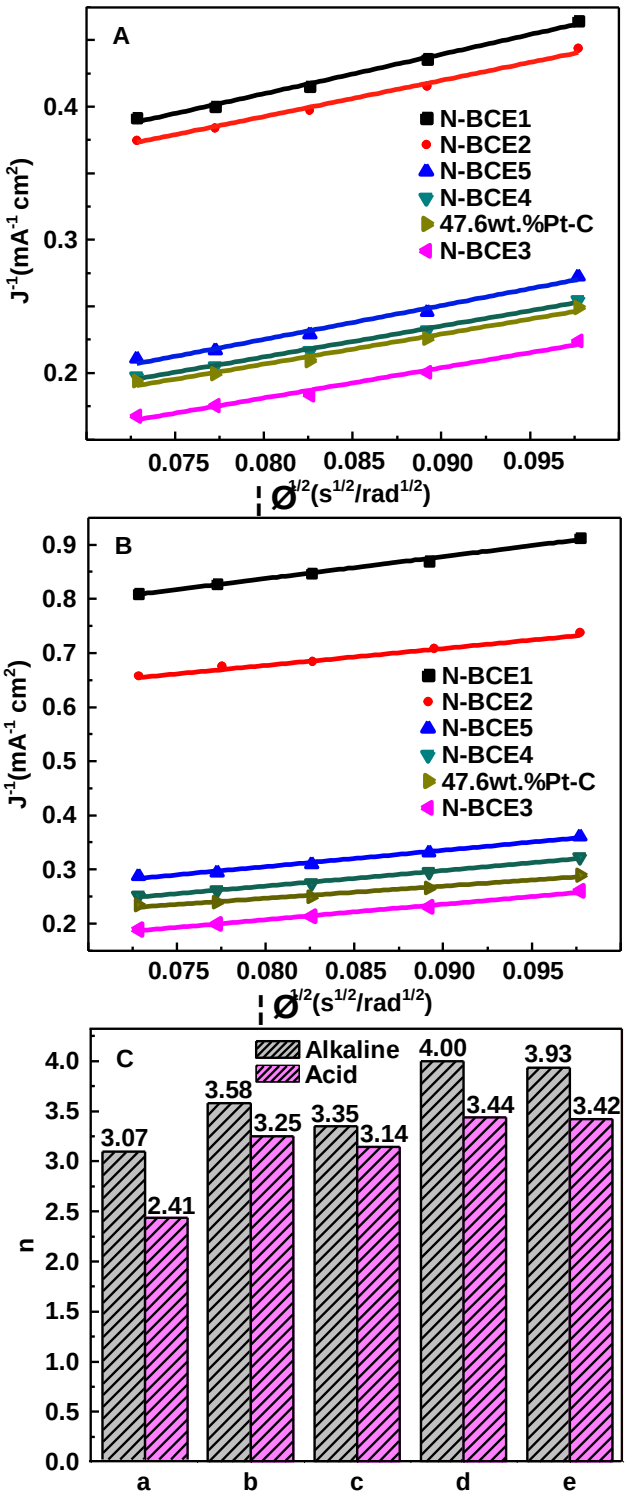

Figure 4. The Koutecky–Levich plots (I^{-1} vs. $\omega^{-1/2}$) of N-BCE1, N-BCE2, N-BCE3, N-BCE4, N-BCE5 and commercial Pt–C catalyst at -0.8 or +0.15 V in O_2-saturated 0.1 M KOH (A) or 1.0 M $HClO_4$ (B) solution and the electron-transfer numbers of N-BCE1 (a), N-BCE5 (b), N-BCE2 (c), N-BCE3 (d) and N-BCE4 (e) in alkaline and acidic media (C).

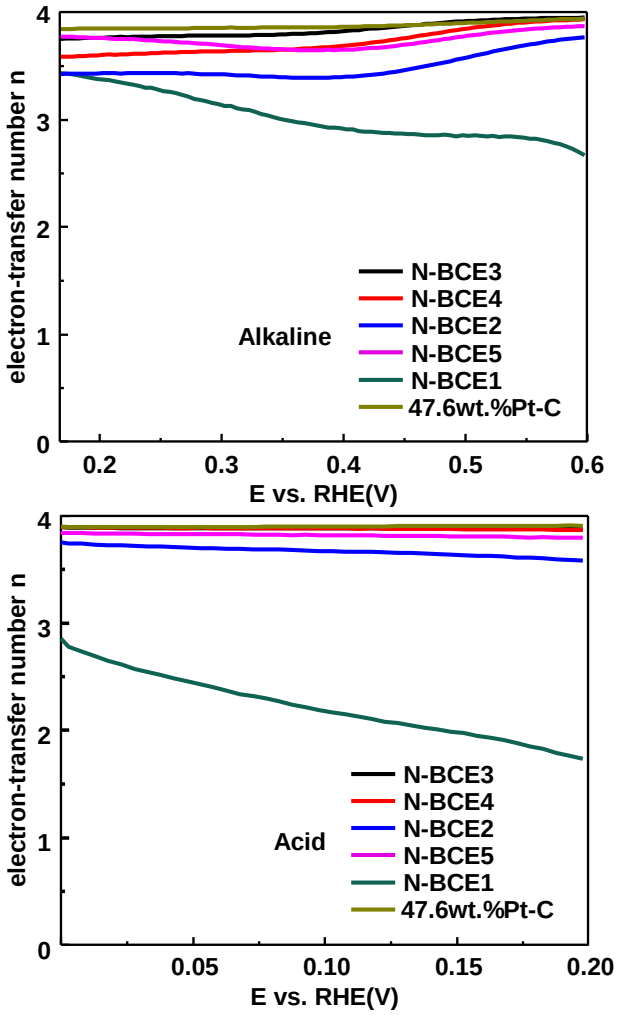

Figure 5. The n values of N-BCE1, N-BCE2, N-BCE3, N-BCE4, N-BCE5 and commercial Pt–C catalyst in O_2-saturated 0.1 M KOH (A) and 1.0 M $HClO_4$ (B) solutions at a rotation speed of 1600.0 rpm.

Moreover, its current densities in the potential ranges from -0.033 to 0.607 V in alkaline medium and from -0.002 to 0.3076 V in acidic medium even surpassed those of the commercial Pt–C catalyst (47.6 wt.%). In addition, N-BCE3 displayed comparable ORR activity when compared with some advanced electrocatalysts (Table 1), further confirming the promising potential of the PW for the preparation of more effective and low-cost ORR electrocatalysts. The superior ORR activity of N-BCE3 is ascribed to its large surface area and high N doping content. Meanwhile, the increased amount of pyridinic N and Fe-N-C also contributed to improve ORR activity, as pyridinic N and Fe-N-C were recently reported to be active sites [32-36].

To better understand the ORR kinetics of the PW-based N-BCEs, LSV tests were also conducted in both oxygen-saturated 0.1 M KOH and 1.0 M $HClO_4$ solutions at different rotation speeds. The electron-transfer number (n) per oxygen molecule was calculated based on the Koutecky-Levich plots at 0.167 V in alkaline medium and at 0.348 V in acidic medium (Fig. 4A-4B).

As seen from Fig. 4C, the n values (4.0, and 3.44; 3.93 and 3.42 in alkaline and acidic media) of N-BCE3 and N-BCE4 were much larger than those (3.07 and 3.35; 3.58 and 2.41; 3.14 and 3.25) of

N-BCE1, N-BCE2 and N-BCE5. These results reveal that the electrocatalytic behaviors on the surfaces of N-BCE3 and N-BCE4 were primarily efficient 4-electron reduction processes, especially for N-BCE3. To further verify the ORR catalytic pathways of these prepared N-BCEs, we also conducted rotating ring disk electrode measurements at 5 mVs^{-1} with a rotation speed of 1600 rpm and a Pt-ring operating potential of 0.5 V. As shown in Fig. 5A-B, the average n value of each prepared sample was in great agreement with the data based on the Koutecky-Levich plots.

For N-BCE3 with superior ORR activity, to estimate its potential for practical application, its durability was investigated by chronoamperometry at a constant voltage of -0.3 V for 30000.0 s in oxygen-saturated 0.1 M KOH and 1.0 M $HClO_4$ solutions. Fig. 6A illustrate that N-BCE3 only lost 3.7 and 8.8 % of the initial current density after 30000.0 s in alkaline and acidic media, respectively, indicating a superior stability compared to the commercial Pt–C catalyst, which displayed 13.0 and 20.4 % current density loss after the same time [17], thus showing the great potential for future applications in acidic and alkaline fuel cells and metal-air batteries.

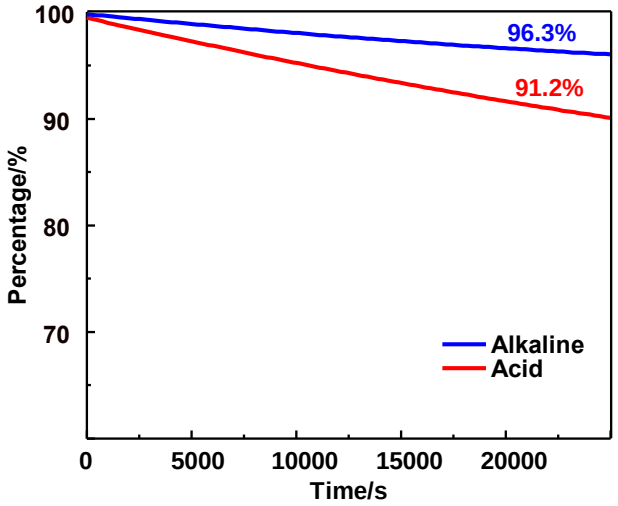

Figure 6. (A) The chronoamperometric response of N-BCE3 in O_2-saturated 0.1 M KOH or 1.0 M $HClO_4$ solution with an oxygen flow rate of 25.0 mL min^{-1} and graphite as the counter electrode at -0.3 or +0.4 V for 30000.0 s.

In addition, it is also interesting that each prepared N-BCE also exhibited much higher OER activity compared to that of the commercial IrO_2 catalyst, evidenced by LSV in nitrogen-saturated 0.1 M KOH or 1.0 M $HClO_4$ solution. In alkaline medium, as shown in Fig. 7A, it is observed that the current density of each N-BCE reached 10.0 mA cm^{-2} at ca. 1.767 V. Among the catalysts, N-BCE3 with a current density of 10.0 mA cm^{-2} at ca. 1.727 V showed much superior OER activity to those of N-BCE1, N-BCE2, N-BCE4 and N-BCE5. Its current densities in the potential range from ca. +1.08 to +1.45 V or ca. +1.83 to +1.87 V were even larger than those of the commercial IrO_2 catalyst. Similarly, in acidic medium, N-BCE3 with a current density of ca. 10.0 mA cm^{-2} at ca. 1.498 V also exhibited the best OER activity (Fig. 7B). In addition, its current densities in the potential range from ca. +0.8 to +1.46 V were also larger than those of the IrO_2 catalyst. Moreover, N-BCE3 even showed more excellent OER activity than some reported catalysts (Table 1), signifying the great promise for applications in unitized regenerative fuel cells and rechargeable metal-air batteries. The superior OER

activity of N-BCE3 indicates that the pyridinic N and Fe-N-C are also the active sites for OER in both alkaline and acidic media [20].

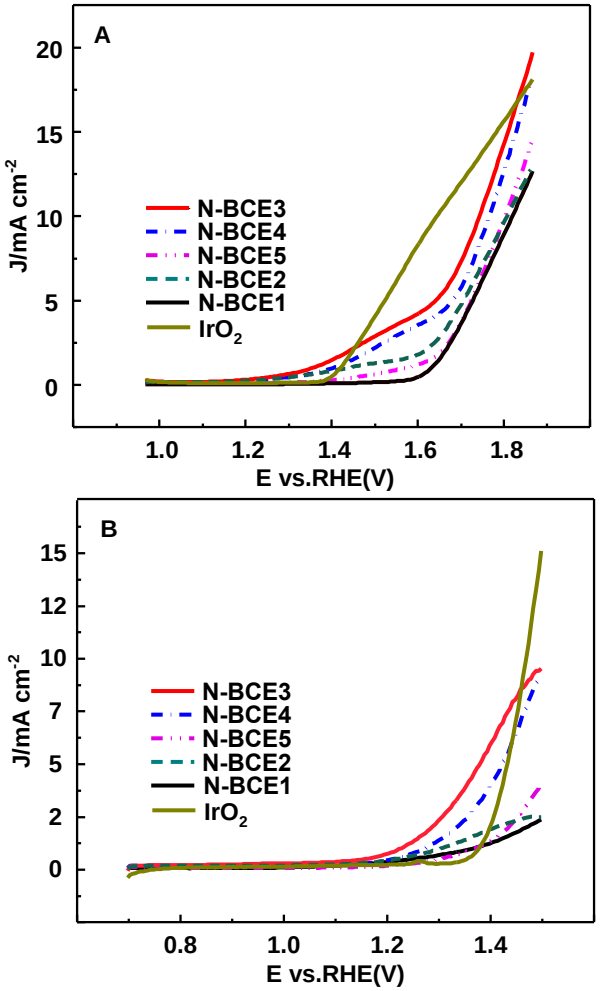

Figure 7. Polarization curves of OER for N-BCE1, N-BCE2, N-BCE3, N-BCE4, N-BCE5 and the commercial IrO_2 catalyst in N_2-saturated 0.1 M KOH (A) or 1.0 M $HCLO_4$ (B) solution at a scan rate of 10.0 mV s^{-1} and rotating speed 1600.0 rpm.

Table 1. The comparison of the ORR and OER activities of N-BCE3 with those of some reported advanced catalysts in alkaline or acidic medium.

Catalyst	Mass loading (mg cm^{-2})	Electrolyte	E_{onset} vs RHE ORR (V)	$E_{1/2}$ vs RHE ORR (V)	E_{OER}(V) (10mA cm^{-2}) (vs, RHE)	Reference
N-BCE3	0.153	0.1 M KOH	0.897 (-0.07 vs Ag/AgCl)	0.767 (-0.2 vs Ag/AgCl)	1.727 (0.76 vs Ag/AgCl)	this work
		1.0 M $HClO_4$	0.658 (0.46 vs Ag/AgCl)	0.49 (0.29 vs Ag/AgCl)	1.498 (1.3 vs Ag/AgCl)	
$N\text{-}OMC_2$	0.153	0.1 M KOH	0.06 vs Ag/AgCl	---	0.76 vs Ag/AgCl	*J. Energy Chem.*, 26 (2017) 422 [20].
		1.0 M	0.56 vs	---	~5.3 mA cm^{-2}	

		$HClO_4$	Ag/AgCl		at 1.3 V	
N-G/CNT	0.43	0.1M KOH	0.88	0.7	1.65	*Angew. Chem. Int. Ed.*, 53 (2014) 6496 [21].
Co/NC-800	0.24	0.1 M KOH	---	-0.19 vs Ag/AgCl	0.93 vs Ag/AgCl	*Mater. Lett.*, 190 (2017) 169 [22].
LO-NF-NCNTS-1.0	0.4	0.1 M KOH	0.896	0.772	~1.73	*Carbon*, 115 (2017) 261 [23].
Co_2P@CoNPG-900	2.0	0.1 M KOH	0.9	0.81	1.728	*Electrochim. Acta*, 231 (2017) 344 [24].
MnO_2-$CoFe_2O_4$/C	0.455	0.1 M KOH	0.85	0.77	1.70	*Appl. Surf. Sci.*, 403 (2017) 51 [25].
Co-N/C-800	0.24	0.1 M KOH	---	0.78	1.74	*J. Mater. Chem. A*, 4 (2016) 16920 [26].
H-Pt/$CaMnO_3$	0.085	0.1 M KOH	---	0.79	1.80	*Adv. Mater.*, 26 (2014) 2047 [27].
NiCoMnO4/N-rGO	0.225	0.1 M KOH	0.92	0.75	~1.74	*Appl. Catal. B*, 201 (2017) 241 [28].
Co-$N_{30\%}$/C-600	0.276	0.1 M KOH	-0.09 vs SCE	---	0.76 vs SCE	*Int. J. Hydrogen Energy*, 41 (2016) 12995 [29].
Co-N/G600	0.24	0.1 M KOH	-0.109 vs Ag/AgCl	---	0.76 vs Ag/AgCl	*Int. J. Hydrogen Energy*, 42 (2017) 5899 [30].
Co@N-PGCS	---	0.1 M KOH	-0.075 vs Ag/AgCl	-0.151 vs Ag/AgCl	0.76 vs Ag/AgCl	*Nanoscale*, 8 (2016) 13311 [31].

4. CONCLUSIONS

In summary, based on cheap PA66 waste, we successfully synthesized a series of N-BCEs. The electrochemical tests demonstrated that the PW-based N-BCE3 exhibited comparable ORR and OER activities to some previously reported advanced heteroatom-doped CEs and transition-metal-based or noble-metal Pt- and Ir-based electrocatalysts in both acidic and alkaline media due to its large surface area, relatively high N doping level and active Fe-N-C species. These results showed that N-containing PW collected from a living environment could be used as a cheap N precursor to fabricate N-doped carbon electrocatalysts with superior ORR and OER activities, showing promising potential application for the development of low-cost and effective ORR and OER catalysts in future fuel cells, metal-air batteries and water oxidation systems, especially in regenerative fuel cells and rechargeable metal-air batteries.

ACKNOWLEDGEMENTS
We acknowledge the financial support from the National Natural Science Foundation of China (No. 21376257), the Jiangsu Provincial Natural Science Foundation of China (No. BK20131112).

References

1. J. T. Zhang, Z. H. Zhao, Z. H. Xia and L. M. Dai, *Nat. Nanotech.*, 10 (2015) 444.
2. G. Chen, D. A. Delafuente, S. Sarangapani, T. E. Mallouk, *Catal. Today*, 67 (2001) 341.
3. Y. Gorlin, T. F. Jaramillo, *J. Am. Chem. Soc.*, 132 (2010) 13612.
4. Y. Zhao, R. Nakamura, K. Kamiya, S. Nakanishi and K. Hashimoto, *Nat. Comm.*, 4 (2013) 2390.
5. W. Wei, H. W. Liang, K. Parvez, X. D. Zhuang, X. L. Feng and K. Mullen, *Angew. Chem. Int. Ed.*, 126 (2014) 1596.
6. H. Zhu, J. Yin, X. L. Wang, H. Y. Wang and X. R. Yang, *Adv. Funct. Mater.*, 23 (2013) 1305.
7. H. R. Zara, S. H. Hashemi and A. Benvidi, *Analy. Chim. Acta*, 668 (2010) 182.
8. S. Ardizzone, G. Fregonara and S. Trasatti, *Electrochim. Acta*, 35 (1990) 263.
9. T. Y. Ma, S. Dai, M. Jaroniec and S. Z. Qiao, *Angew. Chem. Int. Ed.*, 53 (2014) 7281.
10. K. Qu, Y. Zheng, S. Dai and S. Z. Qiao, *Nano Energy*, 19 (2016) 373.
11. S. Chen, J. J. Duan, M. Jaroniec and S. Z. Xiao, *Adv. Mater.*, 26 (2014) 2925.
12. R. Li, Z. D. Wei and X. L. Gou, *ACS Catal.*, 5 (2015) 4133.
13. K. Sakaushi, T. P. Fellinger and M. Antonietti, *ChemSusChem*, 8 (2015) 1156.
14. G. L. Tian, M. Q. Zhao, D. S. Yu, X. Y. Kong, J. Q. Huang, Q. Zhang and F. Wei, *Small*, 10 (2014) 2251.
15. J. Yu, G. Chen, J. Sunarso, Y. L. Zhu, R. Ran, Z. H. Zhu, W. Zhou and Z. P. Shao, *Adv. Sci.*, 3 (2016) 1600060.
16. G. Chen, J. Sunarso, Y. P. Zhu, J. Yu, Y. J. Zhong, W. Zhou and Z. P. Shao, *ChemElectroChem*, 3 (2016) 1760.
17. Z. W. Liu, X. Fu, X. Y. Wei and F. Peng, *J. Mater. Chem. A*, 3 (2015) 22723.
18. H. L. Peng, Z. Y. Mo, S. J. Liao, H. G. Liang, L. J. Yang, F. Luo, H. Y. Song, Y. L. Zhong and B. Q. Zhang, *Sci. Rep.*, 3 (2013) 1765.
19. Z. Y. Guo, G. Y. Ren, C. C. Jiang, X. Y. Lu, Y. Zhu, L. Jiang and L. M. Dai, *Sci. Rep.*, 5 (2015) 17064.
20. M. Li, Z.W .Liu, F. Wang, J. J. Xuan, *J. Energy Chem.*, 26 (2017) 422.
21. Z. H. Wen, S. Q. Ci, Y. Hou, J. H. Chen, *Angew. Chem. Int. Ed.*, 53 (2014) 6496.
22. Q. Wang, X. Qiu, W. H. Hu, Y. M. Huang, *Mater. Lett.*, 190 (2017) 169.
23. Z. J. Wang, F. Zhang, C. Jin, Y. Luo, J. Sui, H. Y. Gong, R. Z. Yang, *Carbon*, 115 (2017) 261.
24. H. Jiang, C. Li, H. B. Shen, Y. S. Liu, W. Z. Li, J. Li, *Electrochim. Acta*, 231 (2017) 344.
25. Y. Wang, Q. Liu, T. J. Hu, L. M. Zhang, Y. Q. Deng, *Appl. Surf. Sci.*, 403 (2017) 51.
26. W. H. Hu, Q. Wang, S. S. Wu, Y. M. Huang, *J. Mater. Chem. A*, 4 (2016) 16920.
27. X. P. Han, F. Y. Cheng, T. R. Zhang, J. G. Yang, Y. X. Hu, *J. Chen, Adv. Mater.*, 26 (2014) 2047.
28. A. Pendashteh, J. Palma, M. Anderson, R. Marcilla, *Appl. Catal. B*, 201 (2017) 241.
29. S. J. Chao, M. J. Geng, *Int. J. Hydrogen Energy*, 41 (2016) 12995.
30. Q. Wang, W. H. Hu, Y. M. Huang, *Int. J. Hydrogen Energy*, 42 (2017) 5899.
31. X. B. Liu, I. S. Amiinu, S. J. Liu, K. Cheng, S. C. Mu, *Nanoscale*, 8 (2016) 13311.
32. D. Guo, R. Shibuya, C. Akiba, S. Saji, T. Kondo and J. Nakamura, *Sci.*, 351 (2016) 361.
33. K. Artyushkova, A. Serov, S. Rojas-Carbonell and P. Atanassov, *J. Phys. Chem. C*, 119 (2015) 217.
34. A. Serov, M. H. Robson, B. Halevi, K. Artyushkova and P. Atanassov, *Electrochem. Commun.*, 22 (2012) 53.
35. G. Wu, K. L. More, C. M. Johnston and P. Zelenay, *Sci.*, 332 (2011) 443.

36. G. Wu and P. Zelenay, *Acc. Chem. Res.*, 46 (2013) 1878.